UNIVERSITÉ DE GENÈVE

Archive ouverte UNIGE
https://archive-ouverte.unige.ch

Article scientifique | Article | 2025

Published version | Open Access

This is the published version of the publication, made available in accordance with the publisher's policy.

Photoreceptor-induced LHL4 protects the photosystem II monomer in *Chlamydomonas reinhardtii*

Dannay, Marie; Bertin, Chloé; Cavallari, Eva; Albanese, Pascal; Tolleter, Dimitri; Giustini, Cécile; Menneteau, Mathilde; Brugière, Sabine; Couté, Yohann; Finazzi, Giovanni; Demarsy, Emilie; Ulm, Roman; Allorent, Guillaume

How to cite

DANNAY, Marie et al. Photoreceptor-induced LHL4 protects the photosystem II monomer in *Chlamydomonas reinhardtii*. In: Proceedings of the National Academy of Sciences of the United States of America, 2025, vol. 122, n° 7, p. e2418687122. doi: 10.1073/pnas.2418687122

This publication URL: https://archive-ouverte.unige.ch/unige:186479
Publication DOI: 10.1073/pnas.2418687122

© The author(s). This work is licensed under a Creative Commons Attribution-NonCommercial-NoDerivatives (CC BY-NC-ND 4.0) https://creativecommons.org/licenses/by-nc-nd/4.0

PNAS RESEARCH ARTICLE | PLANT BIOLOGY OPEN ACCESS

Photoreceptor-induced LHL4 protects the photosystem II monomer in *Chlamydomonas reinhardtii*

Marie Dannay[a,b], Chloé Bertin[a,1], Eva Cavallari[a], Pascal Albanese[a,c], Dimitri Tolleter[a], Cécile Giustini[a], Mathilde Menneteau[a], Sabine Brugière[c], Yohann Couté[c], Giovanni Finazzi[a], Emilie Demarsy[b], Roman Ulm[b,d,2], and Guillaume Allorent[a,2]

Edited by Krishna Niyogi, University of California, Berkeley, CA; received September 12, 2024; accepted January 9, 2025

Photosynthesis, the fundamental process using light energy to convert carbon dioxide to organic matter, is vital for life on Earth. It relies on capturing light through light-harvesting complexes (LHC) in photosystem I (PSI) and PSII and on the conversion of light energy into chemical energy. Composition and organization of PSI and PSII core complexes are well conserved across evolution. PSII is particularly sensitive to photodamage but benefits from a large diversity of photoprotective mechanisms, finely tuned to handle the dynamic and ever-changing light conditions. Light Harvesting Complex protein family members (LHC and LHC-like families) have acquired a dual function during evolution. Members of the LHC antenna complexes of PS capture light energy, whereas others dissipate excess energy that cannot be harnessed for photosynthesis. This process mainly occurs through nonphotochemical quenching (NPQ). In this work, we focus on the Light Harvesting complex-Like 4 (LHL4) protein, a LHC-like protein induced by ultraviolet-B (UV-B) and blue light through UV Resistance locus 8 (UVR8) and phototropin photoreceptor-activated signaling pathways in the model green microalgae *Chlamydomonas reinhardtii*. We demonstrate that alongside established NPQ effectors, LHL4 plays a key role in photoprotection, preventing singlet oxygen accumulation in PSII and promoting cell survival upon light stress. LHL4 protective function is distinct from that of NPQ-related proteins, as LHL4 specifically and uniquely binds to the transient monomeric form of the core PSII complex, safeguarding its integrity. LHL4 characterization expands our understanding of the interplay between light harvesting and photoprotection mechanisms upon light stress in photosynthetic microalgae.

ultraviolet-B | high light | photosynthesis | acclimation

Significance

For photoautotrophs, light is both an essential driver of photosynthesis and a potential threat when in excess. Our research unveils the photoreceptor-induced Light Harvesting complex-Like 4 (LHL4) as a protagonist in the photoprotective response against harmful effects of high light (HL) in *Chlamydomonas reinhardtii*. LHL4 is a critical component of the core of the photosynthetic machinery where it limits the production of damaging molecules, ensuring cell survival under HL. Thus, we provide insights into the molecular and mechanistic strategies employed by photosynthetic microalgae confronted with light stress, improving our understanding of their acclimation responses.

Photosynthetic organisms encounter daily light fluctuations in their natural environments. As light is a source of energy for photosynthesis but can also be a source of photodamage, balancing light absorption and light dissipation is crucial for survival and fitness (1). Photosynthetic organisms have evolved different strategies to acclimate and respond to light fluctuations. These responses include a range of complementary mechanisms collectively known as photoprotection (2). These mechanisms, which are activated at different times in response to light changes, serve to prevent, limit, or repair photodamage (3, 4). For example, dissipation of light energy through nonphotochemical quenching (NPQ) and scavenging of reactive oxygen species (ROS) are activated within minutes, playing crucial roles for survival under excessive light (5–8). Light-Harvesting Complex (LHC) proteins and the related LHC-like proteins have evolved different functions in light absorption and photoprotection from green algae to flowering plants (9). LHC-like family members contain one to four transmembrane domains each harboring putative LHC motifs that may bind chlorophyll a/b, carotenoid, and lipids (9). In algae, including the green microalgae *Chlamydomonas reinhardtii* (abbreviated as Chlamydomonas hereafter), important NPQ effectors are the LHC-Like Stress Related (LHCSR) proteins LHCSR1 and LHCSR3 (10). In vascular plants, where LHCSR proteins are absent, Photosystem II Subunit S (PSBS) is a major player of NPQ (7). PSBS also contributes to NPQ in green microalgae, although to a lesser extent than the LHCSR proteins (11–14). Besides NPQ, plant photoprotection has been proposed to be modulated through the action of the LHC-like Early Light Induced Protein (ELIP) family. ELIPs possibly prevent the negative effect of free chlorophyll molecules released during the turnover of photosystem II (PSII) (15). However, the exact function of other LHC-like proteins remains unknown.

Photoprotective mechanisms are activated by photoreceptors that monitor the light environment (16). In green microalgae, expression of *LHCSR*s, *PSBS*, and *ELIP*s is highly light-inducible through blue light-activated phototropin (PHOT) and UV-B-activated UV Resistance Locus 8 (UVR8) photoreceptors (12, 17, 18). The early steps of UVR8 signaling are well conserved in the green lineage (19, 20), with UV-B-induced UVR8

Author affiliations: [a]Université Grenoble Alpes, CNRS, CEA, INRAE, Interdisciplinary Research Institute of Grenoble, Cell and Plant Physiology Laboratory, Grenoble 38000, France; [b]Department of Plant Sciences, Section of Biology, Faculty of Sciences, University of Geneva, Geneva 1211, Switzerland; [c]Université Grenoble Alpes, CEA, INSERM, UA13 BGE, CNRS, CEA, Grenoble FR2048, France; and [d]Institute of Genetics and Genomics of Geneva, University of Geneva, Geneva 1211, Switzerland

Author contributions: M.D., G.F., E.D., R.U., and G.A. designed research; M.D., C.B., E.C., P.A., D.T., C.G., M.M., S.B., E.D., and G.A. performed research; M.D., C.B., E.C., P.A., D.T., S.B., Y.C., G.F., E.D., R.U., and G.A. analyzed data; and G.F., E.D., R.U., and G.A. wrote the paper.

The authors declare no competing interest.

This article is a PNAS Direct Submission.

Copyright © 2025 the Author(s). Published by PNAS. This open access article is distributed under Creative Commons Attribution-NonCommercial-NoDerivatives License 4.0 (CC BY-NC-ND).

[1]Present address: UMR9019 Genome Integrity & Cancers–CNRS, Université Paris-Saclay, Gustave Roussy Cancer Campus, Villejuif 94800, France.

[2]To whom correspondence may be addressed. Email: roman.ulm@unige.ch or guillaume.allorent@cea.fr.

This article contains supporting information online at https://www.pnas.org/lookup/suppl/doi:10.1073/pnas.2418687122/-/DCSupplemental.

Published February 13, 2025.

monomerization and binding to Constitutively Photomorphogenic 1 (COP1), an E3 ubiquitin ligase playing a vital role in repressing light responses and photomorphogenesis in photosynthetic organisms (12, 21–25). UVR8 binding inhibits COP1, stabilizing transcription factors and thereby leading to transcriptional reprogramming (19, 26–28). In flowering plants, blue light gene expression relies on cryptochrome photoreceptor–COP1 mediated pathway (23, 27, 29), whereas PHOTs seem to control blue light responses independently of early transcriptional changes (30, 31). In contrast, in Chlamydomonas, PHOT induces transcription of *LHCSR3* through a signaling cascade that involves COP1 (also known as LRS1/HIT1) (17, 28, 32, 33). Downstream of COP1, molecular players apparently diverged during evolution. The B-box transcription factor Constans (CrCO) controls *LHCSR*s expression in response to both UV-B and high light (HL) in Chlamydomonas (28, 32), whereas the bZIP transcription factor Elongated Hypocotyl 5 (HY5) plays the major role in the UV-B and blue light signaling pathway in flowering plants (34–38), but its role remains elusive in green algae (39).

Here, we identify the Chlamydomonas LHC-Like protein 4 (LHL4) as a crucial component of the photoprotection response. *LHL4* expression and LHL4 accumulation are strongly induced under UV-B and HL in a UVR8- and PHOT-dependent manner, respectively. Induction involves transcriptional regulation through CrCO. Transcriptomic data corroborate the conclusion that CrCO plays a major role in UVR8-dependent transcriptional reprogramming. Finally, we propose that LHL4-mediated photoprotection prevents ROS production during HL stress by directly interacting with the PSII monomer. The LHL4 protective function is prominent during a first phase of moderate HL stress, i.e. before activation of the canonical NPQ effectors, or when they do not provide sufficient protection under strong HL stress.

Results and Discussion

LHL4 Is Highly Induced upon UV-B. We analyzed the effect of UV-B on the membrane-enriched proteome of Chlamydomonas and identified several proteins potentially involved in photoprotection among those accumulating under 16 h UV-B (Fig. 1*A*). After UV-B exposure, 46 proteins showed a significant increase in abundance, and nine proteins showed a significant decrease in abundance. Several proteins that showed increased accumulation in response to UV-B are involved in PSII biogenesis, stability, or repair [Filamentous Temperature-Sensitive-like H (FTSH-like) and Degradation of periplasmic proteases (40), and members of the High Chlorophyll Fluorescence (HCF) family (41)], as well as in NPQ (the two LHC-like proteins LHCSR1 and LHCSR3) (*SI Appendix*, Table S1). Interestingly, we identified a third LHC-like protein, namely LHL4, enriched more than seven times under UV-B compared to control (Fig. 1*A* and *SI Appendix*, Table S1). In a parallel RNA-Seq analysis, *LHL4* was also identified as highly induced at the transcript level in response to 1 h exposure to UV-B, in a UVR8-dependent manner, along with 831 genes (Fig. 1*B* and *SI Appendix*, Fig. S1 and Table S2). While LHCSRs were detected in both experiments, *PSBS* was identified among the top-induced genes in our transcriptome dataset (*SI Appendix*, Table S2), as expected (12, 25), but showed only limited accumulation at the protein level in the UV-B-treated samples (*SI Appendix*, Table S1), consistent with its reported limited stability over time (11, 14). In total, 44 out of the 46 proteins accumulating in response to UV-B were also found to be transcriptionally induced (Fig. 1*C* and *SI Appendix*, Table S3). LHL4 is a 285-amino acid protein with three predicted transmembrane domains that differs from the other LHC-Like proteins (including the ELIP family) because it contains an exceptionally long predicted loop between the second and third transmembrane domains (Fig. 1*D*) (42, 43). LHL4 homologs are uniquely found in green microalgae (44, 45), where they are closely related to PSBS, but belong to a different clade (Fig. 1*E*).

***LHL4* Expression Is Controlled by UVR8 and PHOT Photoreceptors and Depends on CrCOP1 and CrCO.** *LHL4* gene expression was found to be rapidly and transiently induced in response to both UV-B and HL (Fig. 2*A*) (25, 42, 43). *LHL4* showed a higher induction by UV-B than HL at both transcript and protein levels. The LHL4 protein level rapidly increased up to 4 h and remained stable for 8 h upon both light treatments (Fig. 2*B*). However, the LHL4 abundance rapidly decreased when cells were returned to low light (LL), unlike LHCSR1 and LHCSR3, which level remained stable for at least 8 h posttreatment (Fig. 2*C*) (46).

As *LHL4* expression is induced in response to UV-B and HL, we examined the accumulation of *LHL4* transcripts and LHL4 proteins in *uvr8* and *phot* mutants. UV-B-dependent induction of *LHL4* expression was abolished in the *uvr8* mutant, but not affected in a *phot* mutant (Fig. 2*D*). Consistently, UV-B-induced LHL4 protein accumulation was absent in *uvr8* but comparable to wild type (WT) in *phot* cells (Fig. 2*G*). Under HL, a comparably weak *LHL4* induction was observed in both photoreceptor mutants and WT cells (Fig. 2*D*). However, accumulation of LHL4 protein was reduced in response to HL in the *phot* mutant compared to WT and *uvr8* (Fig. 2*G*), similar to LHCSR3 (*SI Appendix*, Fig. S2*A*) (17). Altogether, our data demonstrate that the induction of LHL4 accumulation by UV-B and HL is mediated by UVR8 and at least partially PHOT, respectively. We thus examined the involvement of downstream signaling components on *LHL4* induction and LHL4 accumulation. We first used the $cop1^{hit1}$ loss-of-function mutant strain that contains an Arg-1256-to-Pro mutation ($CrCOP1^{R1256P}$) in the C-terminal WD40 domain (12, 33). Under both UV-B and HL, the $cop1^{hit1}$ mutant exhibited a much weaker induction of *LHL4* transcripts and reduced LHL4 protein accumulation in comparison to WT (Fig. 2 *E* and *H*). This result is similar to the reduced accumulation of LHCSR1 and LHCSR3 (*SI Appendix*, Fig. S2*B*), as well as PSBS (12), confirming that the UV-B and HL signaling pathways converge at the level of COP1. It is also of note that $cop1^{hit1}$ is more strongly affected in HL-induced LHCSR3 and LHCSR1 accumulation than *phot* (*SI Appendix*, Fig. S2 *A* and *B*), suggesting that additional HL-induced signaling pathway(s) converge at COP1.

We next investigated transcription factors potentially involved in *LHL4* regulation upon UV-B and HL by comparing LHL4 levels in *crco* (28, 32) and *crblz3* [CrBLZ3 is a putative AtHY5 ortholog, (39)] mutants with WT. At the transcriptome-wide level, we found that both CrCO and CrBLZ3 are required for UV-B-regulated gene expression with CrCO playing a major role (*SI Appendix*, Fig. S3 *A* and *B* and Table S2). In agreement, accumulation of *LHL4* mRNA and LHL4 protein in response to both UV-B and HL was severely impaired in *crco* but was similar between *crblz3* and WT (Fig. 2 *F* and *I* and *SI Appendix*, Fig. S2*C* and Table S2). We conclude that UV-B- and HL-dependent accumulation of LHL4 depends on UVR8 and partially on PHOT, respectively, and in both cases involves CrCO-dependent transcriptional activation of *LHL4* expression.

LHL4 Binds the PSII Monomer upon UV-B Exposure. To elucidate the integration of LHL4 within the Chlamydomonas photosynthetic apparatus, we performed biochemical analysis under nondenaturing conditions by Blue native polyacrylamide gel electrophoresis (BN-PAGE) of solubilized thylakoid complexes

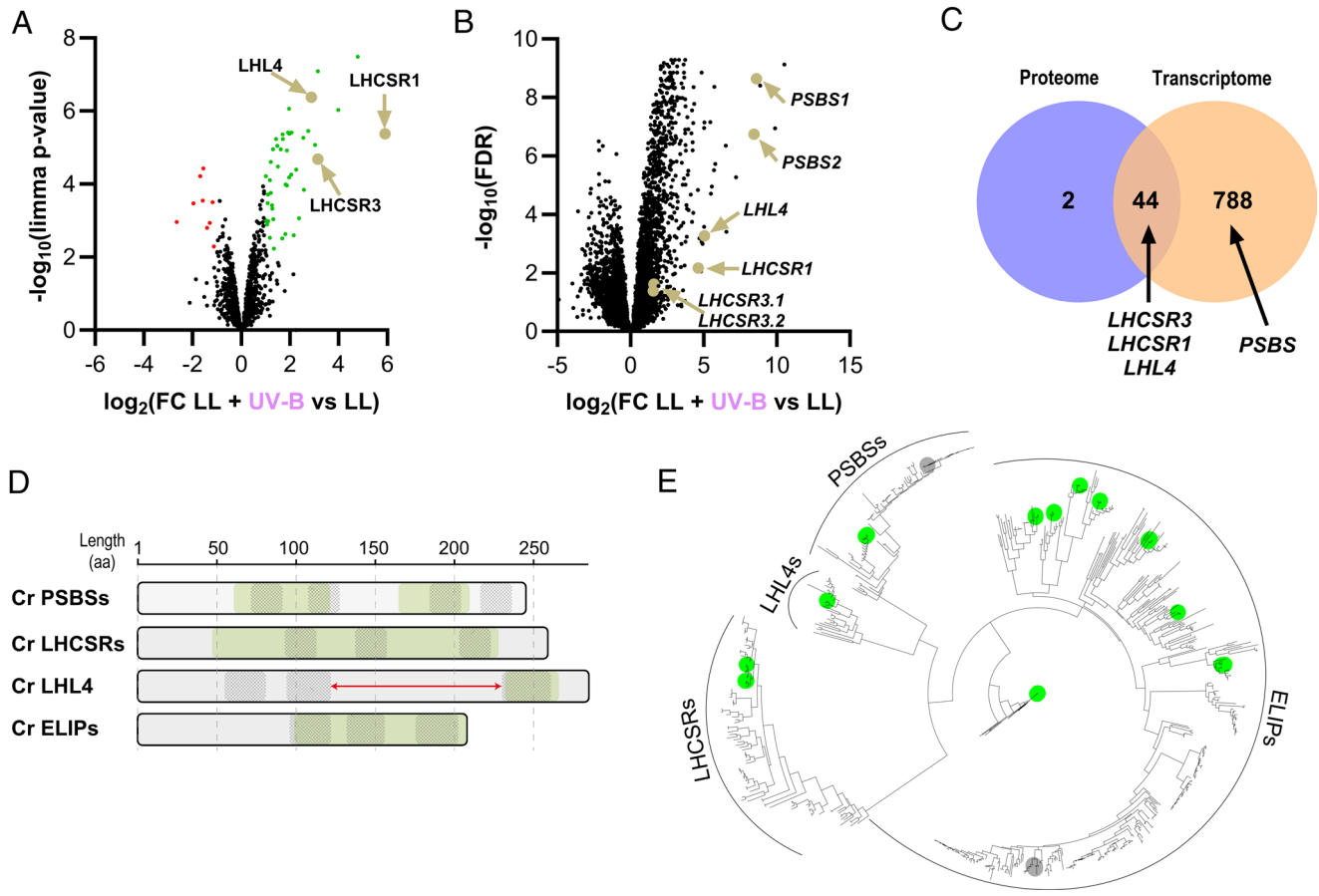

Fig. 1. LHL4 is induced by UV-B in Chlamydomonas. (*A*) Mass spectrometry (MS)-based quantitative comparison of membrane-enriched proteomes from Chlamydomonas exposed to 16 h of supplemental UV-B [Low Light (LL, 20 µmol photons m^{-2} s^{-1}) + UV-B (0.2 mW cm^{-2})] compared to untreated control (LL). Volcano plot displaying the differential abundance of proteins in the membrane proteomes analyzed by MS-based label-free quantitative proteomics. The volcano plot represents the $-\log_{10}$ (*P*-value), (limma *P*-value, *y* axis) plotted against the $\log_2$FC (LL+UV-B vs. LL, *x* axis) for each quantified protein. Green and red dots represent proteins significantly enriched in LL+UV-B and in LL samples, respectively ($\log_2$FC ≥ 1 and $-\log_{10}$(*P*-value) ≥ 2.11, corresponding to a Benjamini–Hochberg FDR < 1%). Dots representing LHL4, LHCSR1, and LHCSR3 proteins are indicated. (*B*) RNA-Seq analysis of Chlamydomonas exposed to 1 h LL+UV-B compared to LL. Volcano plot displaying the differential abundance of transcripts by representing the $-\log_{10}$ (FDR), (*y* axis) plotted against the $\log_2$FC (LL+UV-B vs. LL, *x* axis). Dots representing *LHL4*, *PSBS1/PSBS2* (encoding PSBS), *LHCSR1*, and *LHCSR3.1/LHCSR3.2* (encoding LHCSR3) transcripts are indicated. (*C*) Venn diagram showing the overlap of proteins (blue) and transcripts (orange) significantly enriched in LL+UV-B (*SI Appendix*, Tables S1 and S2). (*D*) Scaled schematic representation of LHC-Like protein sizes and the locations of predicted chlorophyll a/b binding domains (green, predicted using the Superfamily database) and transmembrane domains (gray motifs) in LHL4 and in consensus Chlamydomonas ELIP, LHCSR, and PSBS like protein sequences. The red arrow indicates the presence of an exceptionally long loop in LHL4 compared to the other proteins. aa, amino acids. (*E*) Phylogenetic tree generated from aligned protein sequences of LHC-Like LHCSRs, LHL4s, PSBSs, and ELIPs homologs. Proteins from Chlamydomonas and *Arabidopsis* are approximatively emphasized by green and gray dots, respectively. Due to their proximity, the two ELIP dots for *Arabidopsis* overlap.

isolated from WT cells exposed to UV-B. We found that LHL4 was only detected upon UV-B exposure and migrated in the LHCII trimer region, as well as in two different spots in proximity to the PSII monomer/cytochrome b_6f bands (Fig. 3*A*). We then used complexome profiling (47) to analyze the protein composition of these two spots by cutting this specific region of the gel into six slices and examining their protein content using mass spectrometry (MS) (Fig. 3*B*). LHL4 was found to be localized in two different organizations of the PSII monomer. The lower band (band 5) corresponded to a PSII monomer containing only one of the two core antennae, specifically CP47, known as the RC47 intermediate complex during PSII assembly (48). The upper band (band 1) consisted of the full PSII monomer with both core antennae, CP43 and CP47. LHL4 was also detected in LL-acclimated samples with the same accumulation pattern (Fig. 3*B*), albeit at a much lower level compared to UV-B-acclimated samples. This suggests that a basal level of the protein is also constitutively present within the PSII monomer in nonstressed samples. To identify potential interactions of LHL4 within the PSII monomer, we then used a combination of BN-PAGE and cross-linking MS (XL-MS) analysis. This approach allows capturing protein–protein interaction by creating covalent bonds between amino acids in close proximity and can be directly applied to complexes previously separated via BN-PAGE (49). Importantly, the chemical cross-linking reaction did not produce any noticeable difference on the presence of major photosynthetic complexes (*SI Appendix*, Fig. S4*A*). XL-MS data acquired on these specific gel bands were first validated by mapping the cross-links on known PSII and cytochrome b_6f structures (*SI Appendix*, Fig. S4 *B–D*), where most fall within an acceptable 20 Å distance cut-off (*SI Appendix*, Fig. S4*C*) (50). We detected two cross-links of LHL4 with both CP43 and CP47, these are compatible with two putative positions predicted by using AlphaFold2 multimer (49) (*SI Appendix*, Fig. S5). The distances of these two reproducible cross-links with CP43 and CP47 are of ~12 and ~20 Å, respectively (*SI Appendix*, Fig. S5), thus validating both structural models. Taken together, these data suggest that LHL4 binds to a fully assembled monomer on both inner antennae (Fig. 3*C*), producing a complex at higher molecular weight detected by immunodetection (Fig. 3*A*) and complexome profiling (band 1, Fig. 3*B*). Alternatively, LHL4 may bind to a partially assembled RC47 on CP47 only, resulting in a smaller complex (Fig. 3*A* and band 5 in Fig. 3*B*). In both cases,

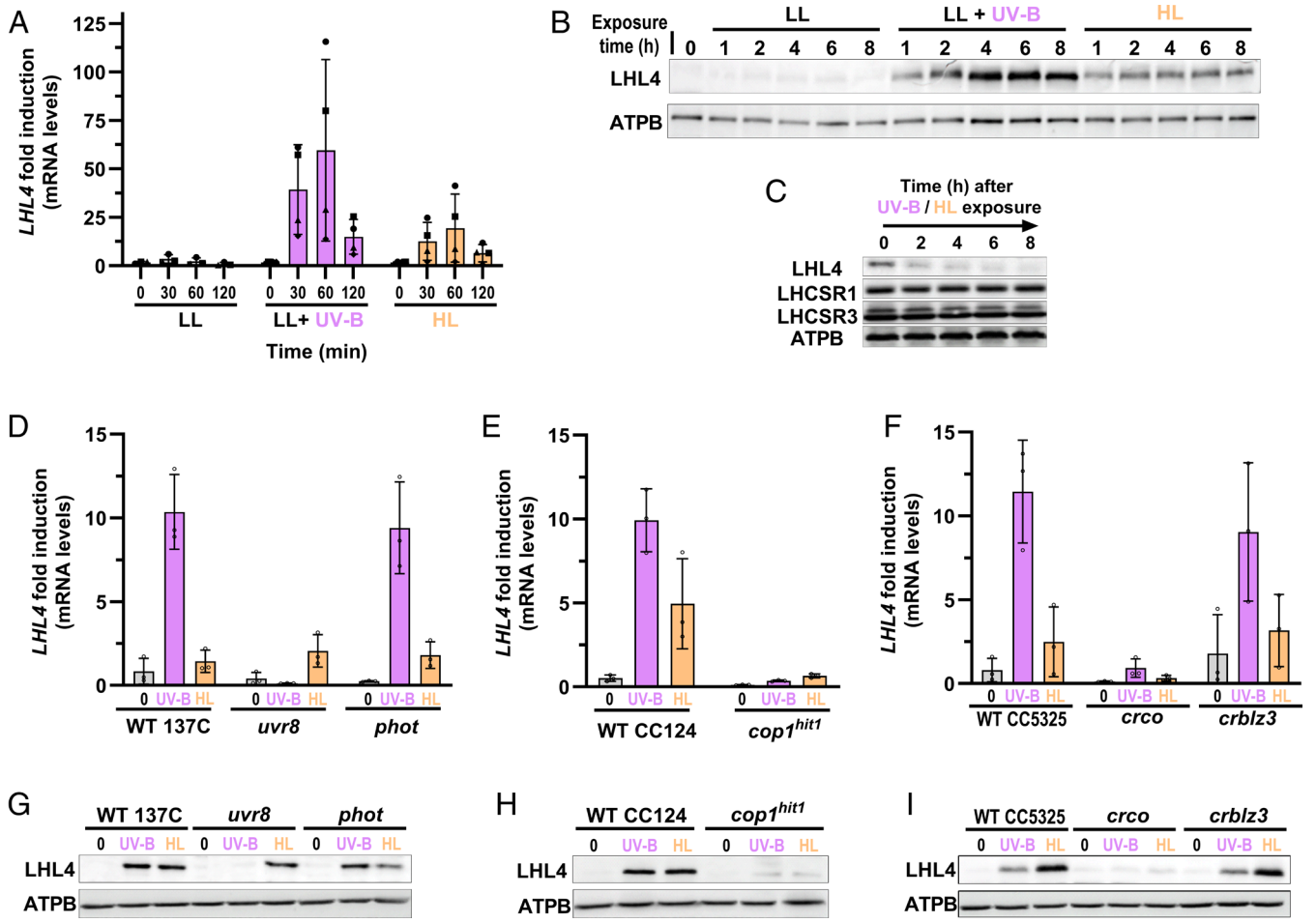

Fig. 2. LHL4 expression is controlled by UVR8 and PHOT photoreceptor signaling pathways. (*A*) RT-qPCR analysis of *LHL4* expression in WT 137C cells grown under LL (20 µmol photons m^{-2} s^{-1}) and then transferred to LL supplemented with UV-B (0.2 mW cm^{-2}, LL+UV-B), or HL (300 µmol photons m^{-2} s^{-1}) for the indicated times. The data were normalized to the *LHL4* levels at time 0 for each condition. Individual data points of biological replicates and means ± SD are shown (n = 4). (*B*) Immunodetection of LHL4 in cells exposed for up to 8 h under LL, LL+UV-B, or HL. ATP synthase beta subunit (ATPB) levels were used as loading control. (*C*) Comparative stability of LHL4 and LHCSRs proteins. Immunodetection of LHL4, LHCSR1, LHSCR3, and ATPB in cells sequentially exposed to LL (20 µmol photons m^{-2} s^{-1}) supplemented with UV-B (0.2 mW cm^{-2}) for 16 h and then HL (300 µmol photons m^{-2} s^{-1}) for 4 h. Cells were finally placed under LL (20 µmol photons m^{-2} s^{-1}) for the indicated times. ATPB was used as loading control. (*D–F*) RT-qPCR analysis of *LHL4* expression in (*D*) *uvr8* and *phot*, (*E*) *cop1*^{hit1}, and (*F*) *crco* and *crblz3* cells grown under LL (0), or exposed for 1 h to LL+UV-B, or HL. Data are normalized to levels in respective WTs (strains 137C, CC124, CC5325) under LL ("0"). Values of independent measurements and means ± SD are shown (n = 3). (*G–I*) Immunodetection of LHL4 in *uvr8* and *phot*, (*H*) *cop1*^{hit1}, (*I*) *crco* and *crblz3*, as well as their respective WT cells grown under LL (0), or 6 h LL+UV-B, or HL. ATPB was used as loading control.

LHL4 binds to the site where the second PSII monomer attaches, suggesting that the protein may need to be removed prior to dimer assembly. We propose that LHL4 acts as or is a part of a specific antenna for the PSII monomer, capable of binding to the complex early in its assembly process by a direct connection to the two core antenna proteins CP43 and CP47.

LHL4 Prevents PSII Photoinhibition upon Exposure to HL. The sequence homology of LHL4 with LHCSR and PSBS, its accumulation in response to both UV-B and HL, as well as its location within the PSII monomer may suggest a role for LHL4 in photoprotection. To investigate this possibility, we generated *lhl4* knock-out mutants using CRISPR-Cas9 and evaluated their tolerance to HL compared to WT. LL-acclimated cells were exposed to HL (900 µmol photons m^{-2} s^{-1}) for 1 h, followed by 1 h of recovery under LL. Their photosynthetic capacity was monitored as the maximum quantum yield of PSII (F_v/F_m). Lower F_v/F_m values indicate, but are not limited to, PSII damage due to photoinhibition (51). *lhl4* mutants showed no difference in PSII antenna size compared to WT (*SI Appendix*, Fig. S6) but exhibited impaired recovery from light stress (Fig. 4 *A* and *B*). To further characterize the role of LHL4, we conducted parallel experiments using lincomycin to inhibit the synthesis of chloroplast-encoded proteins of PSII, effectively blocking its repair system. Upon lincomycin treatment, we assume that recovery is linked to reversibly photodamaged PSII, as suggested before (52). On the contrary, the additional recovery observed without the inhibitor likely reflects irreversible photodamaged PSII, which can only be repaired via assembly of de novo synthesized PSII proteins (52). As expected, we observed a significant reduction in the recovery of both strains compared to untreated samples upon addition of lincomycin. While the inhibition rate was the same, a large difference in the recovery between WT and *lhl4* became evident (Fig. 4 *A* and *B*). This finding rules out a direct role for LHL4 in the repair process, in agreement with a parallel report (53). Instead, it implies a role of LHL4 in PSII recovery from light-mediated degradation, which would stem from increased pool of reversibly photodamaged PSII. By binding to the PSII monomer at the core antenna subunits CP43 and CP47, we propose that LHL4 might protect the PSII monomer pool from degradation during HL. This could help preserve its structural integrity and facilitate the assembly of functional PSII dimers, leading to a more efficient recovery.

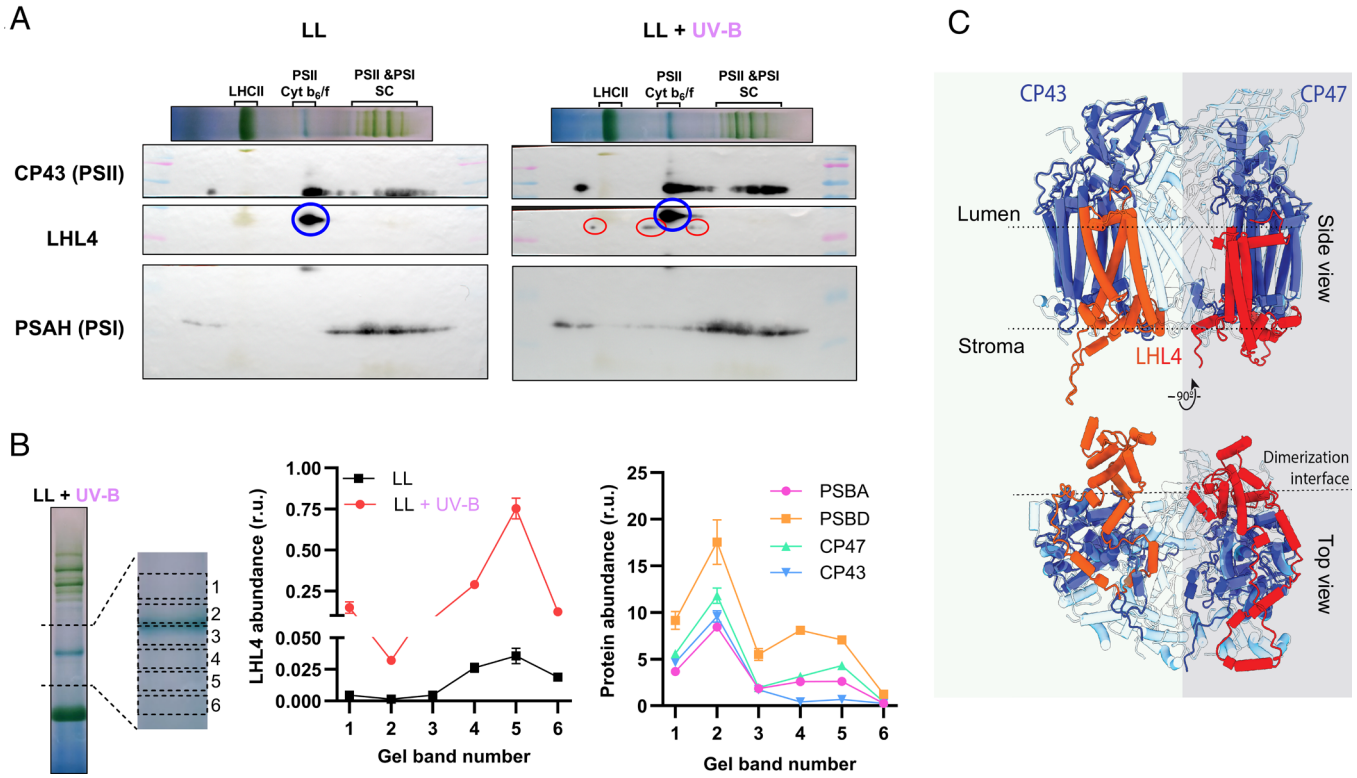

Fig. 3. LHL4 localizes with PSII monomers at the dimerization interface interacting with the inner PSII antenna proteins CP43 and CP47. (*A*) BN-PAGE of thylakoids extracted from cells exposed to LL (20 µmol photons m^{-2} s^{-1}) or LL supplemented with UV-B (LL +UV-B; 0.2 mW cm^{-2}). Second dimension blots indicate LHL4 (red circles), and its absence in LL cells. A blue circle indicates a nonspecific band detected by the LHL4 antibody in both WT and *lhl4*. (*B*) The middle section of the gel was divided into six parts, as shown in the *Left* image. The relative abundance of LHL4 (*Left* graph) and the main components of the PSII monomer (*Right* graph; UV-B acclimated cells) were assessed by MS. n = 4 (*C*) LHL4 interactors CP43 and CP47 uncovered by cross-linking and in-gel digestion of the BN-PAGE band. The two AlphaFold2 pairwise predictions of LHL4-CP43/47 are shown overlaid on the PSII monomer structure (PDB 6KAD, light blue) and both are localized at the dimerization interface.

A defect in photoprotection generally leads to ROS production during photosynthesis, mainly singlet oxygen ($^1O_2$) at the PSII level (8). We measured $^1O_2$ levels in WT and *lhl4* during HL exposure (Fig. 4*C*). During early HL exposure (20 min), i.e., when LHL4 expression is still very low (Fig. 3*B*), $^1O_2$ levels are comparable in both strains. However, we observed a significant overaccumulation of $^1O_2$ in the *lhl4* strain compared to the WT under prolonged stress, while LHL4 accumulated at a higher level in the WT (Fig. 4*C*). Our data suggest that the protection of PSII monomers by LHL4 facilitates PSII renewal and helps limiting photoinhibition and $^1O_2$ production. Accordingly, in case of higher (2,000 µmol photons m^{-2} s^{-1}) and prolonged light stress exposure, in contrast to WT, *lhl4* cultures were unable to survive, resulting in complete bleaching within 2 h of exposure (Fig. 4*D*).

To cope with the harmful effects of light stress, photosynthetic organisms can activate NPQ. We investigated the interplay between the NPQ-driven and LHL4-mediated protection. First, we monitored the phenotype of LHL4 during the first 3 h of HL exposure. During this phase, cells begin to accumulate the LHCSR3 protein, which is responsible for NPQ activity (54, 55). We observed a stable difference in the recovery between WT and *lhl4* cells during the first 2 h of HL (*SI Appendix*, Fig. S7*A*). At this point, NPQ became activated to a similar extent in both strains (*SI Appendix*, Fig. S7*B*). This observation suggests that LHL4 does not directly contribute to this process in Chlamydomonas. Alternatively, NPQ capacity could compensate, at least partially, the absence of protection conferred by LHL4 in the mutant. After 3 h of exposure, NPQ was highly activated, leading to a higher Fv/Fm and similar fluorescence recovery between the two strains. Overall, these results suggest that LHL4 primarily catalyzes a recovery from light stress when cells have not yet developed their NPQ capacity.

We further dissected the impact of NPQ on LHL4-mediated protection, focusing on UV-B acclimated cells that had fully developed their NPQ capacity (*SI Appendix*, Fig. S7*C*). We observed that LHL4 accumulation in UV-B-acclimated cells was significantly lower after 1 h of HL exposure compared to LL-acclimated cells (*SI Appendix*, Fig. S7*D*). Additionally, the *lhl4* strain showed no significant difference in Fv/Fm compared to the WT during the first hour of light stress and subsequent recovery, which was significantly higher than in nonacclimated cells (*SI Appendix*, Fig. S7 *E* and *F*). These results confirm that when cells have acquired NPQ capacity, energy dissipation via NPQ prevents photoinhibition, reducing PSII damage and turnover, and limits LHL4 induction, which is not essential under these conditions. We further evaluated the impact of LHL4 under long-term exposure and stronger HL intensity (2,000 µmol photons m^{-2} s^{-1}) in UV-B acclimated samples. Under these conditions, LHL4 levels are maintained at a very high level (*SI Appendix*, Fig. S7*G*). Both WT and *lhl4* cells retained their green pigmentation longer than LL-acclimated cells (*SI Appendix*, Fig. S7*H* vs. Fig. 4*D*). However, after 8 h of prolonged exposure, *lhl4* failed to endure the stress and bleached, whereas the WT cells remained green (*SI Appendix*, Fig. S7*H*). These results suggest that under prolonged and extremely high irradiance, NPQ alone is no longer sufficient to prevent photodamage. Therefore, the cumulative effect over time of the absence of PSII monomers-driven LHL4 protection affects cell survival. This complementary role of NPQ and LHL4 in these extreme conditions underscores the importance of LHL4 in

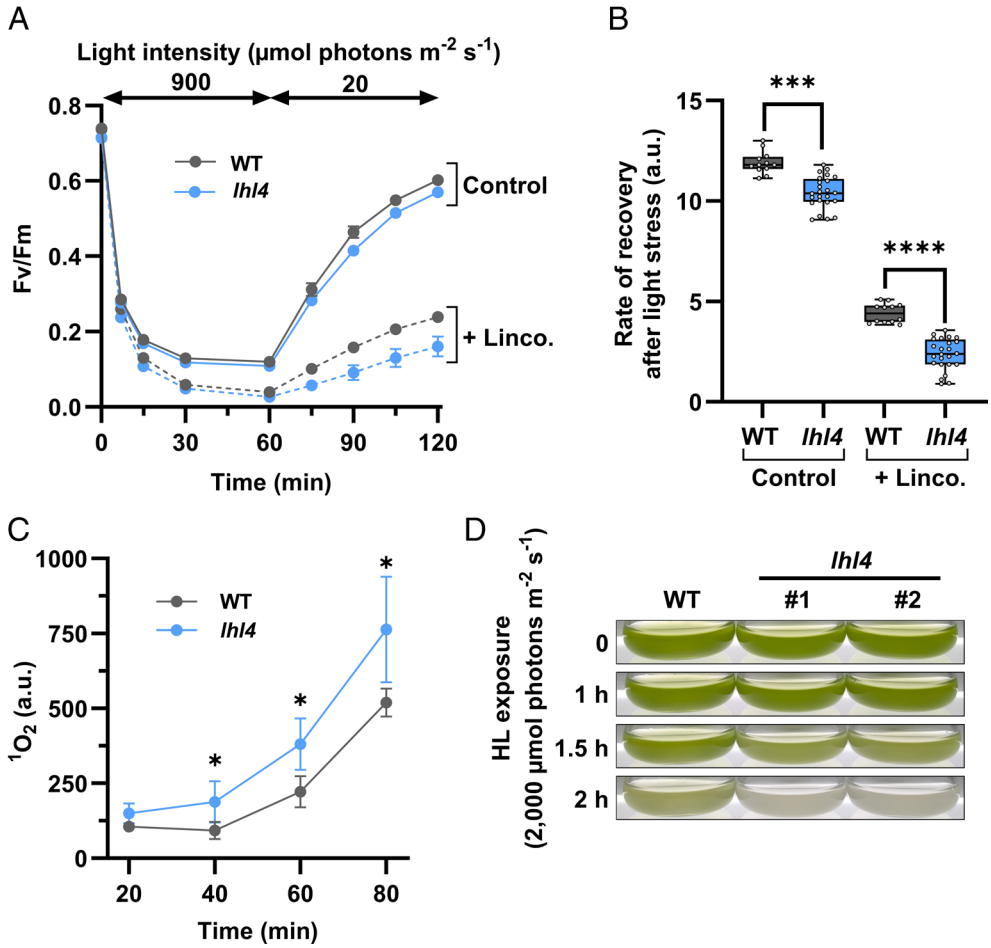

Fig. 4. LHL4 protects PSII and facilitates cell survival under HL. WT and *lhl4* cells were grown under LL (20 µmol photons m^{-2} s^{-1}). (*A*) Cells were exposed to HL (900 µmol photons m^{-2} s^{-1}) for 1 h and then placed under LL for 1 h and their maximum PSII quantum yield (Fv/Fm) was monitored after 1 min of dark relaxation. The data presented are representative of four biological replicates. Errors bars represent the SE of the means of three technical replicates. (*B*) The rate of recovery was calculated using the data from panel *A* by determining the slope of the first 30 min of recovery under LL and 1 min of dark relaxation. n = 4. The asterisk indicates statistical difference (***$P < 0.001$, ****$P < 0.0001$). (*C*) WT and *lhl4* cells were exposed to HL (600 µmol photons m^{-2} s^{-1}, red light) and $^1O_2$ accumulation was monitored over 80 min of exposure. n = 3. Asterisks indicate statistical differences (*$P < 0.05$). (*D*) Photographs of WT and *lhl4* cultures were taken after LL acclimation (0) and then after 1, 1.5, and 2 h under 2,000 µmol photons m^{-2} s^{-1}.

priming UV-B-induced photoprotection in *Chlamydomonas*, alongside LHCSRs (12).

Conclusion

Our study reveals a key role for the LHL4 protein in photoprotection. LHL4 protects PSII monomers by associating with the core complex via two antenna proteins, CP43 and CP47. This protection takes place during the early stages of photodamage upon HL exposure, but also under prolonged stress conditions when light intensity is too high. Protection conferred by LHL4 occurs following cell exposure to UV-B and HL, which concomitantly activate the UVR8 and PHOT photoreceptor signaling pathways that converge likely at the COP1 level in Chlamydomonas. Our phylogenetic analysis indicates that LHL4 is exclusively present in green microalgae. However, its crucial function in photoprotection of these organisms suggests the existence of similar actors in other phototrophs. Consistently, specific High-Light-Inducible Proteins (HLIPs) have been identified in cyanobacteria, where they associate with CP47 and intermediates of PSII assembly modules (56). Remarkably, cyanobacteria lacking HLIPs are viable but experience extreme light-induced stress levels, suggesting the presence of protective mechanism in prokaryotic photosynthetic organisms similar to the one conferred by Chlamydomonas LHL4. Investigating potential candidates in other microalgae and flowering plants may unlock a deeper understanding of photoprotection mechanisms across diverse photosynthetic life forms.

Materials and Methods

Algae Strains. Chlamydomonas mutant strains *lhl4* (LHL4^{K34*}; * indicating a translation stop codon), *uvr8* (UVR8^{S86*}), and *phot* (PHOT^{C32*}) were generated in the WT137C parental strain (55) (*SI Appendix*, Fig. S8) by introducing a TAA STOP codon by homology-directed repair using CRISPR-Cas9 (57, 58). The following target sequences were used: 5′-CGTGTCAACGCCGAGAAAAG-3′ for *lhl4*, 5′-CGAGGACAGATCTACAGCTG-3′ for *uvr8*, and 5′-CACGCTTCCGGACTGTCCGC-3′ for *phot*. The following templates for DNA repair were used: 5′-CGCAGTG ATTGCCCGTGTCAACGCCGAGAAtataaggaccacgacatcgactacaaggacAAGTGGC TTTGCAAAGGTAAGCTGAGAACT-3′ for *lhl4*, 5′-GGTCGCGTCGTCACGAGGACAGATCTAC AGtataaggaccacgacatcgactacaaggacCTGGGGCTGGTGGGTGGCGTTGGGGCGCAG-3′ for *uvr8*, and 5′-TCGTCGCAGATGCCACGCTTCCGGACTGTCtataaggaccacgacatcgact acaaggacCGCTGGTCTACGCCAGCGAGGGGTGAGCGG-3′ for *phot*. The *cop1*^{hit1} mutant is in the CC124 WT background (33). *crco* (LMJ.RY402.149321) (28, 32) and *crblz3* (LMJ.RY402.194448) (39) mutants were obtained from the Chlamydomonas Library Project (CLiP) (59) together with their corresponding WT (CC5325). *uvr8* (LMJ.RY40202.156289) (12) from the CLiP library was used for the RNA-seq experiment.

Algae Culture and Light Treatment. Algae cells were grown in Tris Acetate Phosphate growth medium (60) under continuous light (20 µmol photons m^{-2} s^{-1}, from white Light Emitting Diode (LED) panels), 25 °C, and shaking (110 rpm).

In all experiments, cells were harvested during the exponential phase (2 to 3 × 10^6 cells per mL), washed, and resuspended in High Salt Medium minimal growth medium at 4.5 × 10^6 cells per mL, with the exception of Fig. 4*D* where they were resuspended at 6 × 10^6 cells per mL. Cells were placed for at least 1 h under dim light (20 μmol photons m^{-2} s^{-1}) before applying specific light treatments. UV-B-exposed samples (+UV-B) were treated by Philips TL20W/01S narrowband UV-B tubes filtered with a WG filter (Schott Glaswerke) with half-maximal transmission at 311 nm (0.07 or 0.2 mW cm^{-2}) (61). Control (−UV-B) samples were placed under a WG filter with half-maximal transmission at 360 nm to block UV-B. In both conditions, samples were concomitantly exposed to dim light (20 μmol photons m^{-2} s^{-1}) provided by fluorescent white light tubes (Osram Dulux L). Cells were exposed to UV-B for 6 h, with the exception of Fig. 1*A* and *SI Appendix*, Fig. S7 *C–H*, where the treatment duration was extended to 16 h to fully induce the UV-B protection of the photosynthetic machinery, as detailed in ref. 12. For HL treatment, cells were placed under white LED panels (SL 3500, Photon Systems Instruments) at the indicated light intensity.

Phylogenetic Analysis. The sequences of LHL4, PSBS1, LHCSR3.1, and ELIP1-9 were subjected to a blastp analysis using the online tool available at https://www.ncbi.nlm.nih.gov/ with a percent identity range of 35 to 100% and a query coverage range of 50 to 100%. Protein sequences were then aligned using the Multiple Alignment using Fast Fourier Transform tool (auto strategy, https://mafft.cbrc.jp/alignment/server/). To enhance the accuracy of the alignment, manual curation was performed using Jalview to eliminate any duplicate or misaligned sequences. The phylogenetic tree was constructed using IQ-TREE, employing the LG+F+I+G4 model. The generated tree was then visualized graphically using iTOL v7, a web-based tool accessible at https://itol.embl.de/.

Protein Extraction and Immunoblot Analysis. Cells were pelleted and resuspended in 80% (v/v) acetone. Proteins were precipitated by centrifugation at 4 °C and resuspended in lysis buffer [100 mM Tris-HCl, pH 6.8, 4% (v/v) SDS, 20 mM Ethylenediaminetetraacetic acid (EDTA)] supplemented with protease inhibitor (cOmplete, Roche). 10 to 30 μg of proteins were separated by SDS-PAGE in Tris-Glycine buffer (25 mM Tris, 190 mM glycine, 0.05% Sodium Dodecyl Sulfate (SDS)), transferred onto nitrocellulose membrane using the same buffer supplemented with 20% (v/v) ethanol for 80 min at 110 V. Anti-CrUVR8 (25), anti-PHOT (17), anti-LHCSR3 (AS142766; Agrisera), anti-LHCSR1 (AS142819; Agrisera), anti-LHL4 (AS07250, Agrisera), anti-ATPB (AS05085; Agrisera), anti-CP43 (AS111787; Agrisera), and anti-PSAH (AS06143; Agrisera) were used in this study. Detection was carried out with an Horseradish Peroxydase -conjugated secondary antibody, and the signal was developed using the Clarity Western ECL Substrates kit (Biorad). Images of the blots were captured using a Charge-Coupled Device imager.

RNA Extraction. Cells were prepared as described above. 20 million cells were then pelleted and frozen in liquid nitrogen. RNA were extracted using the RNeasy Plant Mini Kit (Qiagen) including a DNase treatment to remove residual genomic DNA (RNase-Free DNase Set, Qiagen).

Quantitative Real-Time PCR (qRT-PCR). cDNA synthesis was performed with the TaqMan Reverse Transcription Reagents kit (Applied Biosystems). Amplification by RT-qPCR was performed using complementary DNA (cDNA) in the presence of SYBR Green (Master Mix PCR Power SYBR™, Applied Biosystems) and specific primers (0.3 μM) for the amplification of the gene of interest, using a CFX Connect Real-Time PCR Detection System (Biorad). Data were analyzed using the ΔΔCt method (62) and the Cre06.g278222_4532 reference gene (25, 63). The following primers were used: 5′- TACGGTGTGGATGACGTGAC-3′ and 5′- AGGTGATAATCTGGCGGATG-3′ for *LHL4* and 5′- CTTCTCGCCCATGACCAC-3′ and 5′- CCCACCAGGTTGTTCTTCAG-3′ for Cre06.g278222_4532.

RNA-seq Analysis. Cells of WT CC-5325, *uvr8*, *crco*, and *crblz3* were exposed for 1 h to LL (20 μmol photons m^{-2} s^{-1}; −UV-B control samples) or LL supplemented with 0.2 mW cm^{-2} of UV-B (+UV-B). Total RNA was extracted from 20 million cells of three independent biological replicates. The RNA quality control, library preparation using TruSeqHT Stranded mRNA (Illumina), and sequencing on an Illumina HiSeq 4000 System using 100-bp single-end reads protocol were performed at the iGE3 genomics platform of the University of Geneva. Quality control was performed with FastQCv.0.11.9. Reads were mapped to the Chlamydomonas genome CreinhardtiiCC_4532_707_v6.1 (PhytozomeV13) using STARv.2.7.10b software (64), with average alignment of 91.65%. Raw counts were obtained using HTSeq v.0.11.3 (65). Filtering out lowly expressed genes (13,613 genes were kept), normalization and differential expression analysis were performed with the R/Bioconductor package edgeR v.3.42.4 (66), and statistical significance was assessed with a general linear model, negative binomial distribution, and quasi-likelihood F test. Genes with a fold change ≥2 and *P*-value ≤ 0.05 [with a multiple testing Benjamini and Hochberg False Discovery Rate (FDR) correction] were considered differentially expressed. Annotations (v6.1) were obtained from the Phytozome database (v13). The RNA-Seq data reported have been deposited in the NCBI Gene Expression Omnibus (www.ncbi.nlm.nih.gov/geo) and are accessible through GEO Series accession number GSE255943.

ROS Quantification. $^1O_2$ production was estimated using the Singlet Oxygen Sensor Green (SOSG, Invitrogen) dye (67). Cultures at 3 × 10^6 cells/mL were placed in 24-well plates. 0.5 μM of SOSG was added to each well, before exposure for 80 min to red light (630 nm, 600 μmol photons m^{-2} s^{-1}, equivalent to 900 μmol photons m^{-2} s^{-1} white light in our condition). This wavelength minimizes photobleaching of the dye, which is sensitive to blue light and prolonged exposure to high-intensity illumination (68). The fluorescence of each well was then measured with a plate reader (Infinite M1000; Tecan) (λ excitation: 504 nm; λ emission: 525 nm ± 5 nm).

NPQ, Photoinhibition, and Antenna Size Measurements. Chlorophyll fluorescence was imaged in 100 μL of cell suspension in a 96-well plate. Fluorescence was quantified using a Speedzen III fluorescence imaging setup (JBeam Bio). Maximum fluorescence in the dark (F_m) or during actinic light exposure ($F_{m'}$, 900 μmol photons m^{-2} s^{-1}) was measured using saturating red pulses (250 ms, 3,000 μmol photons m^{-2} s^{-1} at 630 nm) followed by blue light (470 nm) detection pulses (10 μs). NPQ was calculated as $(F_m - F_{m'})/F_{m'}$ (69). For photoinhibition experiments, cells were treated in 24-well plates for 1 h with HL (white light, 900 μmol photons m^{-2} s^{-1}) and then placed under LL for 1 h (20 μmol photons m^{-2} s^{-1}). Lincomycin was added at a final concentration of 1.2 mM to inhibit chloroplast translation when needed. The chlorophyll fluorescence was then measured before (F_0) and right after the saturating pulse (F_m), and the maximum quantum yield of PSII was calculated as $F_v/F_m = (F_m - F_0)/F_m$. Antenna size was measured under different light intensity after addition of 10 μM of [(3-(3,4-dichlorophenyl)-1,1-dimethylurea] and estimated as the half-time to reach F_m level (70, 71). Samples were dark adapted for at least 10 min for NPQ (55) and antenna size experiments, 1 min for photoinhibition experiments (52).

MS-Based Proteomic Analyses. Three biological replicates of Chlamydomonas cells exposed or not to UV-B for 16 h were prepared. The Chlamydomonas cells were disrupted in a tube containing glass beads using a Precellys instrument (Bertin Technologies) at 7,500 rpm and 4 °C for two cycles of 30 s each, with a 30-s pause in between. Subsequently, the samples were centrifuged at 20,000 g for 5 min at 4 °C. The resulting pellets, enriched with membrane proteins, were resuspended in a solution containing 50 mM Tris-HCl pH 6.8, 2% SDS, 10 mM EDTA, and protease inhibitor (cOmplete, Roche) to maintain the integrity of the proteins during further processing. Proteins were then solubilized in buffer (72) and heated for 10 min at 95 °C. They were then stacked in the top of a 4 to 12% NuPAGE gel (Invitrogen), stained with Coomassie blue R-250 (Bio-Rad) before in-gel digestion using modified trypsin (Promega, sequencing grade) as previously described (73). The resulting peptides were analyzed by online nanoliquid chromatography coupled to MS/MS (Ultimate 3000 RSLCnano and Q-Exactive HF, Thermo Fisher Scientific) using a 120-min gradient. For this purpose, the peptides were sampled on a precolumn (300 μm × 5 mm PepMap C18, Thermo Scientific) and separated in a 75 μm × 250 mm C18 column (Reprosil-Pur 120 C18-AQ, 1.9 μm; Maisch GmbH). The MS and MS/MS data were acquired using Xcalibur version 2.9 (Thermo Fisher Scientific).

Peptides and proteins were identified by Mascot (version 2.8.0, Matrix Science) through concomitant searches against the Chlre5_6 databases [downloaded from JGI Genome Portal, (74), 19,526 sequences], the mitochondrion and chloroplast protein sequences (downloaded from NCBI, respectively 69 and 8 proteins), and a homemade database containing the sequences of classical contaminant proteins found in proteomic analyses (human keratins, trypsin, … 126 sequences). Trypsin/P was chosen as the enzyme and two missed cleavages were allowed. Precursor and fragment mass error tolerances were set respectively at 10 and 20 ppm. Peptide modifications allowed during the search were Carbamidomethyl (C, fixed), Acetyl (Protein N-term, variable), and Oxidation (M, variable). The Proline software [version 2.2.0, (75)] was used for the compilation, grouping,

and filtering of the results [conservation of rank 1 peptides, peptide length ≥ 6 amino acids, FDR of peptide-spectrum-match identifications < 1% (76), and minimum of one specific peptide per identified protein group]. Proline was then used to perform a MS1 label-free quantification of the identified protein groups based on razor and specific peptides.

Statistical analysis was performed using the ProStaR software (77) based on the quantitative data obtained with the three biological replicates analyzed per condition. Proteins identified in the contaminant database, proteins identified by MS/MS in less than two replicates of one condition, and proteins quantified in less than three replicates of one condition were discarded. After log2 transformation, abundance values were normalized using the variance stabilizing normalization method, before missing value imputation (Sparse Low-Rank Sequence Alignment algorithm for partially observed values in the condition and DetQuantile algorithm for totally absent values in the condition). Statistical testing was conducted with limma, whereby differentially expressed proteins were selected using a $\log_2$FC cut-off of 1 and a *P*-value cut-off of 0.00776, allowing to reach a FDR inferior to 1% according to the Benjamini–Hochberg estimator. Proteins found differentially abundant but identified by MS/MS in less than two replicates or detected in less than three replicates in the condition in which they were found to be more abundant were manually invalidated (*P*-value = 1).

Thylakoid Isolation and BN-PAGE. 400 million cells were broken in a 2 mL tube containing glass beads using a Precellys instrument (Bertin Technologies) at 7,500 rpm and 4 °C for two cycles of 30 s each, with a 30-s pause in between. The lysate was diluted in 25 mM HEPES pH 7.5, 5 mM $MgCl_2$, 0.3 M sucrose, and protease inhibitor (cOmplete, Roche) and then centrifuged at 20,000 g for 5 min at 4 °C. The pellet was resuspended in 1 mM HEPES pH 7.5, 5 mM EDTA, and 0.3 M sucrose and centrifuged again at the same speed. Thylakoids were isolated using a discontinuous three-step sucrose gradient (1.8 M, 1.3 M, 0.5 M) after centrifugation (76,000 g, 1 h, 4 °C). The chlorophyll concentration was estimated, and 20 μg of chlorophyll was solubilized in 1% α-dodecylmaltoside for 5 min at room temperature. For the BN-PAGE analysis, a loading buffer (0.5 M aminocaproic acid, 30% sucrose, 100 mM Bis-Tris HCl pH 7, and 50 mg/mL blue Coomassie G-250) was added to the sample. The thylakoid extract was then loaded onto a 4 to 16% NativePAGE (InVitrogen), and gel electrophoresis was conducted with increasing voltage intensity (ranging from 75 V to 200 V) in an anode buffer (50 mM Bis-Tris HCl pH 7) and a blue cathode buffer (50 mM Tricine, 15 mM Bis-Tris HCl pH 7, and 0.01% blue Coomassie G-250). When the migration reached the middle of the gel, the blue buffer was replaced with fresh cathode buffer devoid of Coomassie blue.

Cross-Linking MS and Structural Modeling. UV-B-treated and untreated (control) cells were disrupted in a tube containing glass beads using a Precellys instrument (Bertin Technologies) at 7,500 rpm and 4 °C for two cycles of 30 s each, with a 30-s pause in between. Cell lysates were chemically cross-linked with 8 mM 4-(4,6-dimethoxy-1,3,5-triazin-2-yl)-4-methyl-morpholinium chloride (DMTMM) for 30 min at 4 °C in the darkness). We used the water-soluble DMTMM reagent because of the scarce availability of exposed Lys residues in the loops of LHL4. DMTMM is considered as a "short-range" cross-linker, lacking a spacer arm and with reactive groups targeting carboxylic acids and primary amines (aspartic and glutamic acids to lysine and amino termini of proteins). This reagent provides distance constraints between 0 and ~25 Å considering the flexibility of the side chains (7 and 5 Å for lysine and carboxylic acids, respectively), the α-carbon backbone (6 Å), and the overall protein flexibility (50, 78). Cross-linked thylakoids were purified according to established protocols and then solubilized for BN-PAGE as described above. Comparison of cross-linked and non-cross-linked thylakoids showed no noticeable differences in the band patterns, we thus assumed the XL reaction did not produce artifacts (*SI Appendix*, Fig. S4). The entire region where the LHL4 antibody was giving a signal on the second dimension from three technical replicates was excised (Fig. 3*A*) and carefully divided into six pieces of ~1 mm. The bands were then subjected to in-gel digestion and MS acquisition as for the proteomic analyses in order to precisely quantify the protein comigrating in these different regions. For the in-gel cross-linking, the entire region was washed rapidly in milliQ water, and soaked for 30 min in 5 mM 4-(2-hydroxyethyl)-1-piperazineethanesulfonic acid (Hepes) pH 7.5, 10 mM EDTA pH 8, and 1.3 M sucrose supplemented with 16 mM DMTMM cross-linker. The cross-linking reaction was then quenched with 10 mM Tris-HCl for 10 min and in-gel digested with the same procedure as for the proteomic analysis (73). Briefly, Liquid Chromatography (LC) separation gradients were of 180 min with elution gradient profiles as follows: 0 to 10% solvent B (0.1% (v/v) formic acid in 80% (v/v) acetonitrile) over 10 min, 12 to 35% solvent B over 125 min, 36 to 44% solvent B over 20 min, 45 to 100% solvent B over 10 min, and finally 100% B for 15 min. Full-scan MS spectra were collected in a mass range of m/z 350 to 1,300 Th in the Orbitrap at a resolution of 60,000 at m/z = 200 Th after accumulation to an Automatic Gain Control (AGC) target value of 1e6 with a maximum injection time of 50 ms. In-source fragmentation was activated and set to 15 eV. The cycle time for the acquisition of MS/MS fragmentation scans was set to 2 s. Charge states accepted for MS/MS fragmentation were set to 3 to 8. Dynamic exclusion properties were set to n = 1 and to an exclusion duration of 15 s. Stepped Higher energy Collision Dissociation fragmentation (MS/MS) was performed with increasing normalized collision energy (27, 30, 33%) and the mass spectra acquired in the Orbitrap at a resolution of 30,000 at m/z = 200 Th after accumulation to an AGC target value of 1e5 with an isolation window of m/z = 1.4 Th and maximum injection time of 120 ms. Additionally, LHL4-containing BN-PAGE bands were acquired with a MS method similar to that used for normal tryptic peptides as described above in order to screen proteins present in the BN-PAGE band.

Raw data were searched using pLink2 (79) for cross-linked peptide pairs or as described above for normal peptide search. A minimal peptide length of six and two miss cleaved sites was allowed. Cysteine carbamidomethylation was set as fixed modification. Methionine oxidation, protein N-term acetylation, and lysine acetylation were set as dynamic modifications. For cross-linked peptides, the reference database containing only the proteins identified from the normal peptide was used, but with an increased number of missed cleavages allowed of 3. Identified cross-links were only accepted through at 1% FDR filter and if present in both replicates.

Cross-links identified were mapped using the ChimeraX plugin XMAS (80) on the PSII monomer (extrapolated from PDB #6KAD) and Cyt b6f (PDB #1Q90) structures. The predicted LHL4 AlphaFold2 model downloadable from UniprotKB was used. For additional validation of the interaction, we docked in parallel LHL4 for the core complex on the HADDOCK webserver (81), using the identified cross-links as distance constraints and predicting the pairwise interaction between CP43/CP47 and LHL4 with Alphafold2 multimer algorithm in ColabFold (82).

For BN-PAGE complexome profiling, the raw LC–MS/MS data were processed using the MS-Fragger (v4.0) (83) integrated into the FragPipe GUI (v21.1). The search was performed against the Chlre5_6 databases [downloaded from JGI Genome Portal, (74), 19,526 sequences]. An integrated contaminant database was used to assign common contaminant proteins. For search, enzyme specificity was set to Trypsin/P (C-terminal cleavage of lysine and arginine) with up to two missed cleavages. The minimal peptide length was set to seven and the maximal peptide mass was set to 6,000 Da. For peptide search, fixed carbamidomethylation of cysteine and up to two variable modifications per peptide were allowed, namely: methionine oxidation and protein N-terminal acetylation. For the database search, precursor and fragment ions mass error was set to 10 and 20 ppm, respectively. Match between runs was allowed within a retention time window of 0.5 min. A FDR of 1% for peptide spectrum matches and proteins was applied. The output result file was further processed to normalize protein abundances on the total intensity of the identified peptides in each run.

Accession Numbers. Sequence data from this article can be found in the Joint Genome Institute Phytozome data libraries (https://phytozome.jgi.doe.gov/pz/portal.html) under the accession numbers (Chlamydomonas genome v6.1) *LHL4*, Cre17.g740950_4532. *UVR8*, Cre05.g230600_4532. *PHOT*, Cre03.g199000_4532. *COP1*, Cre02.g085050_4532. *CrCO*, Cre06.g278159_4532. *CrBLZ3*, Cre06.g310500_4532. *LHCSR1*, Cre08.g365900_4532. *LHCSR3*, Cre08.g367500_4532 and Cre08.g367400_4532. *PSBS*, Cre01.g016600_4532 and Cre01.g016750_4532, *ELIP1*, Cre14.g626750_4532. *ELIP2*, Cre16.g679250_4532. *ELIP3*, Cre02.g143550_4532. *ELIP4*, Cre07.g320400_4532. *ELIP5*, Cre04.g211850_4532. *ELIP7*, Cre08.g384650_4532. *ELIP8*, Cre09.g393173_4532. *ELIP9*, Cre09.g394325_4532. *RACK1*, Cre06.g278222_4532.

Data, Materials, and Software Availability. All MS raw data files, including the search results (spectral matches and the cross-link tables), are deposited to the ProteomeXchange Consortium via the PRIDE partner repository (dataset identifier PXD048496 (84) for the bottom–up proteomics data, PXD055508 (85)

for the BN-PAGE complexome profiling data, and PXD049352 (86) for the XL-MS data). The RNA-Seq data reported in this article have been deposited in the NCBI Gene Expression Omnibus and are accessible through GEO Series accession number GSE255943 (87). The two AlphaFold2 predictions and the combinatory PDB model showing the two predicted interacting positions of LHL4 are available as a Zenodo public repository deposition (https://zenodo.org/records/14262714) (88).

ACKNOWLEDGMENTS. We thank Olaf Kruse for kindly providing the *cop1*^{hit1} mutant and Michel Goldschmidt-Clermont and Stéphane Ravanel for helpful discussions throughout the project. We thank Anja Krieger-Liszkay for technical discussions regarding ROS measurements and Caroline Juery, Yamama Naciri, and Charles Pouchon for their assistance in conducting the phylogenetic analysis of LHL4. We also thank Florence Courtois, Gilles Curien, and Michel Goldschmidt-Clermont for their critical reading of the manuscript. The RNA-Seq experiments were performed at the Institute of Genetics and Genomics of Geneva, Genomics Platform of the University of Geneva (https://ige3.genomics.unige.ch/), and we thank Natacha Civic and Céline Delucinge Vivier for bioinformatic analysis. This work was supported by an Initiative d'excellence (IDEX) Université Grenoble Alpes International Strategic Partnership grant (project Signalling UV-B to protect Photosynthesis), the University of Geneva, and, in part, by the Swiss NSF (grant 310030_207716 to R.U.). P.A. acknowledges funding from the European Union's Horizon 2020 research and innovation programme under the Marie Skłodowska-Curie grant agreement No. 101066400–PHOTO-LINK. C.G. and G.F. acknowledge funding from the European Research Council ERC (Chloro-Mito; grant no. 833184). C.B. and G.A. acknowledge funding from the CNRS Momentum program. This work is also supported by the French National Research Agency (ANR) in the framework of the "Investissements d'avenir" program (ANR-15-IDEX-02) and by Grenoble Alliance for Structural Biology (GRAL), a program from the Chemistry Biology Health Graduate School of University Grenoble Alpes (ANR-17-EURE-0003) (E.C., Y.C., G.F., and G.A.). Proteomic experiments were partially supported by ANR under projects Proteomics French Infrastructure (ANR-10-INBS-08).

1. A. Gjindali, G. N. Johnson, Photosynthetic acclimation to changing environments. *Biochem. Soc. Trans.* **51**, 473–486 (2023).
2. K. K. Niyogi, Photoprotection revisited: Genetic and molecular approaches. *Annu. Rev. Plant Biol.* **50**, 333–359 (1999).
3. H.-S. Jung, K. K. Niyogi, "Molecular analysis of photoprotection of photosynthesis" in *Photoprotection, Photoinhibition, Gene Regulation, and Environment*, B. Demmig-Adams, W. W. Adams, A. K. Mattoo, Eds. (Springer, 2008), pp. 127–143.
4. E. Erickson, S. Wakao, K. K. Niyogi, Light stress and photoprotection in *Chlamydomonas reinhardtii*. *Plant J.* **82**, 449–465 (2015).
5. K. K. Niyogi, T. B. Truong, Evolution of flexible non-photochemical quenching mechanisms that regulate light harvesting in oxygenic photosynthesis. *Curr. Opin. Plant Biol.* **16**, 307–314 (2013).
6. A. V. Ruban, Nonphotochemical chlorophyll fluorescence quenching: Mechanism and effectiveness in protecting plants from photodamage. *Plant Physiol.* **170**, 1903–1916 (2016).
7. X. P. Li *et al.*, A pigment-binding protein essential for regulation of photosynthetic light harvesting. *Nature* **403**, 391–395 (2000).
8. B. B. Fischer, É. Hideg, A. Krieger-Liszkay, Production, detection, and signaling of singlet oxygen in photosynthetic organisms. *Antioxid. Redox Signal.* **18**, 2145–2162 (2013).
9. J. D. Rochaix, R. Bassi, LHC-like proteins involved in stress responses and biogenesis/repair of the photosynthetic apparatus. *Biochem. J.* **476**, 581–593 (2019).
10. R. Arshad *et al.*, A kaleidoscope of photosynthetic antenna proteins and their emerging roles. *Plant Physiol.* **189**, 1204–1219 (2022).
11. T. Tibiletti, P. Auroy, G. Peltier, S. Caffarri, *Chlamydomonas reinhardtii* PsbS protein is functional and accumulates rapidly and transiently under high light. *Plant Physiol.* **171**, 2717–2730 (2016).
12. G. Allorent *et al.*, UV-B photoreceptor-mediated protection of the photosynthetic machinery in *Chlamydomonas reinhardtii*. *Proc. Natl. Acad. Sci. U.S.A.* **113**, 14864–14869 (2016).
13. S. Wilson, E. Kim, A. Ishii, A. V. Ruban, J. Minagawa, Overexpression of LHCSR and PsbS enhance light tolerance in *Chlamydomonas reinhardtii*. *J. Photochem. Photobiol. B* **244**, 112718 (2023).
14. V. Correa-Galvis *et al.*, Photosystem II Subunit PsbS Is involved in the induction of LHCSR Protein-dependent energy dissipation in *chlamydomonas reinhardtii*. *J. Biol. Chem.* **291**, 17478–17487 (2016).
15. I. Adamska, M. Roobol-Bóza, M. Lindahl, B. Andersson, Isolation of pigment-binding early light-inducible proteins from pea. *Eur. J. Biochem.* **260**, 453–460 (1999).
16. E. Demarsy, M. Goldschmidt-Clermont, R. Ulm, Coping with 'Dark Sides of the Sun' through photoreceptor signaling. *Trends Plant Sci.* **23**, 260–271 (2018).
17. D. Petroutsos *et al.*, A blue-light photoreceptor mediates the feedback regulation of photosynthesis. *Nature* **537**, 563–566 (2016).
18. G. Allorent, D. Petroutsos, Photoreceptor-dependent regulation of photoprotection. *Curr. Opin. Plant Biol.* **37**, 102–108 (2017).
19. R. Podolec, E. Demarsy, R. Ulm, Perception and signaling of Ultraviolet-B radiation in plants. *Annu. Rev. Plant Biol.* **72**, 793–822 (2021).
20. Z. Zhang *et al.*, Origin and adaptive evolution of UV RESISTANCE LOCUS 8-mediated signaling during plant terrestrialization. *Plant Physiol.* **188**, 332–346 (2022).
21. R. Tokutsu, K. Fujimura-Kamada, T. Yamasaki, K. Okajima, J. Minagawa, UV-A/B radiation rapidly activates photoprotective mechanisms in *Chlamydomonas reinhardtii*. *Plant Physiol.* **185**, 1894–1902 (2021).
22. X. Han, X. Huang, X. W. Deng, The photomorphogenic central repressor COP1: Conservation and functional diversification during evolution. *Plant Commun.* **1**, 100044 (2020).
23. R. Podolec, R. Ulm, Photoreceptor-mediated regulation of the COP1/SPA E3 ubiquitin ligase. *Curr. Opin. Plant Biol.* **45**, 18–25 (2018).
24. A. Oravecz *et al.*, CONSTITUTIVELY PHOTOMORPHOGENIC1 is required for the UV-B response in Arabidopsis. *Plant Cell* **18**, 1975–1990 (2006).
25. K. Tilbrook *et al.*, UV-B perception and acclimation in *chlamydomonas reinhardtii*. *Plant Cell* **28**, 966–983 (2016).
26. J. J. Favory *et al.*, Interaction of COP1 and UVR8 regulates UV-B-induced photomorphogenesis and stress acclimation in Arabidopsis. *EMBO J.* **28**, 591–601 (2009).
27. K. Lau, R. Podolec, R. Chappuis, R. Ulm, M. Hothorn, Plant photoreceptors and their signaling components compete for COP 1 binding via VP peptide motifs. *EMBO J.* **38**, e102140 (2019).
28. R. Tokutsu, K. Fujimura-Kamada, T. Matsuo, T. Yamasaki, J. Minagawa, The CONSTANS flowering complex controls the protective response of photosynthesis in the green alga Chlamydomonas. *Nat. Commun.* **10**, 4099 (2019).
29. J. Ponnu, T. Riedel, E. Penner, A. Schrader, U. Hoecker, Cryptochrome 2 competes with COP1 substrates to repress COP1 ubiquitin ligase activity during Arabidopsis photomorphogenesis. *Proc. Natl. Acad. Sci. U.S.A.* **116**, 27133–27141 (2019).
30. J. M. Christie, Phototropin blue-light receptors. *Annu. Rev. Plant Biol.* **58**, 21–45 (2007).
31. M. Ohgishi, K. Saji, K. Okada, T. Sakai, Functional analysis of each blule light receptor, cry1, cry2, phot1, and phot2, by using combinatorial multiple mutants in arabidopsis. *Proc. Natl. Acad. Sci. U.S.A.* **101**, 2223–2228 (2004).
32. S. T. Gabilly *et al.*, Regulation of photoprotection gene expression in Chlamydomonas by a putative E3 ubiquitin ligase complex and a homolog of CONSTANS. *Proc. Natl. Acad. Sci. U.S.A.* **116**, 17556–17562 (2019).
33. L. Schierenbeck *et al.*, Fast forward genetics to identify mutations causing a high light tolerant phenotype in *Chlamydomonas reinhardtii* by whole-genome-sequencing. *BMC Genomics* **16**, 57 (2015).
34. Y. Xiao *et al.*, HY5: A pivotal regulator of light-dependent development in higher plants. *Front. Plant Sci.* **12**, 800989 (2022).
35. M. T. Osterlund, C. S. Hardtke, W. Ning, X. W. Deng, Targeted destabilization of HY5 during light-regulated development of Arabidopsis. *Nature* **405**, 462–466 (2000).
36. M. Binkert *et al.*, UV-B-Responsive association of the Arabidopsis bZIP transcription factor ELONGATED HYPOCOTYL5 with target genes, including its own promoter. *Plant Cell* **26**, 4200–4213 (2014).
37. B. A. Brown *et al.*, A UV-B-specific signaling component orchestrates plant UV protection. *Proc. Natl. Acad. Sci. U.S.A.* **102**, 18225–18230 (2005).
38. R. Ulm *et al.*, Genome-wide analysis of gene expression reveals function of the bZIP transcription factor HY5 in the UV-B response of Arabidopsis. *Proc. Natl. Acad. Sci. U.S.A.* **101**, 1397–1402 (2004).
39. N. Lämmermann *et al.*, Ubiquitin ligase component LRS1 and transcription factor CrHy5 act as a light switch for photoprotection in Chlamydomonas. bioRxiv [Preprint] (2020). https://doi.org/10.1101/2020.02.10.942334 (Accessed 12 February 2020).
40. Y. Zou, P. V. Bozhkov, Chlamydomonas proteases: Classification, phylogeny, and molecular mechanisms. *J. Exp. Bot.* **72**, 7680–7693 (2021).
41. M. Plöchinger, S. Schwenkert, L. Von Sydow, W. P. Schröder, J. Meurer, Functional update of the auxiliary proteins PsbW, PsbY, HCF136, PsbN, TerC and ALB3 in maintenance and assembly of PSII. *Front. Plant Sci.* **7**, 423 (2016).
42. H. Teramoto *et al.*, Action spectrum for expression of the high intensity light-inducible Lhc-like gene Lhl4 in the green alga *Chlamydomonas reinhardtii*. *Plant Cell Physiol.* **47**, 419–425 (2006).
43. H. Teramoto, T. Itoh, T. A. Ono, High-intensity-light-dependent and transient expression of new genes encoding distant relatives of light-harvesting chlorophyll-a/b proteins in *Chlamydomonas reinhardtii*. *Plant Cell Physiol.* **45**, 1221–1232 (2004).
44. I. Grouneva *et al.*, Phylogenetic viewpoints on regulation of light harvesting and electron transport in eukaryotic photosynthetic organisms. *Planta* **237**, 399–412 (2013).
45. J. Razeghi, A. Kianianmomeni, UV-B response is modulated by cell-type specific signaling pathway in multicellular green algae *Volvox carteri*. *Plant Growth Regul.* **87**, 303–315 (2019).
46. W. J. Nawrocki, X. Liu, R. Croce, *Chlamydomonas reinhardtii* exhibits de facto constitutive NPQ capacity in physiologically relevant conditions. *Plant Physiol.* **182**, 472–479 (2020).
47. B. Spaniol *et al.*, Complexome profiling on the Chlamydomonas lpa2 mutant reveals insights into PSII biogenesis and new PSII associated proteins. *J. Exp. Bot.* **73**, 245–262 (2022).
48. H. S. Mehra *et al.*, Assembly and repair of photosystem II in *Chlamydomonas reinhardtii*. *Plants* **13**, 811 (2024).
49. J. F. Hevler *et al.*, Selective cross-linking of coinciding protein assemblies by in-gel cross-linking mass spectrometry. *EMBO J.* **40**, e106174 (2021).
50. A. Leitner *et al.*, Chemical cross-linking/mass spectrometry targeting acidic residues in proteins and protein complexes. *Proc. Natl. Acad. Sci. U.S.A.* **111**, 9455–9460 (2014).
51. N. R. Baker, Chlorophyll fluorescence: A probe of photosynthesis in vivo. *Annu. Rev. Plant Biol.* **59**, 89–113 (2008).
52. A. Nordhues *et al.*, Evidence for a role of VIPP1 in the structural organization of the photosynthetic apparatus in Chlamydomonas. *Plant Cell* **24**, 637–659 (2012).
53. J. Lang *et al.*, Complexome profiling of the Chlamydomonas psb28 mutant reveals THYLAKOID ENRICHED FRACTION 5 as an early photosystem II assembly factor. bioRxiv. [Preprint] (2024). https://doi.org/10.1101/2024.06.24.600430 (Accessed 29 June 2024).
54. G. Peers *et al.*, An ancient light-harvesting protein is critical for the regulation of algal photosynthesis. *Nature* **462**, 518–521 (2009).
55. G. Allorent *et al.*, Dual strategy to cope with high light in *Chlamydomonas reinhardtii*. *Plant Cell* **25**, 545–557 (2013).
56. J. Komenda, R. Sobotka, Cyanobacterial high-light-inducible proteins–Protectors of chlorophyll-protein synthesis and assembly. *Biochim. Biophys. Acta* **1857**, 288–295 (2016).
57. A. Greiner *et al.*, Targeting of photoreceptor genes in *Chlamydomonas reinhardtii* via zinc-finger nucleases and CRISPR/Cas9. *Plant Cell* **29**, 2498–2518 (2017).
58. S. Kelterborn *et al.*, Gene editing in green alga *Chlamydomonas reinhardtii* via CRISPR-Cas9 ribonucleoproteins. *Methods Mol. Biol.* **2379**, 45–65 (2022).

59. X. Li *et al.*, An indexed, mapped mutant library enables reverse genetics studies of biological processes in *chlamydomonas reinhardtii*. *Plant Cell* **28**, 367–387 (2015).
60. J. Kropat *et al.*, A revised mineral nutrient supplement increases biomass and growth rate in *Chlamydomonas reinhardtii*. *Plant J.* **66**, 770–780 (2011).
61. L. Rizzini *et al.*, Perception of UV-B by the arabidopsis UVR8 protein. *Science* **332**, 103–106 (2011).
62. K. J. Livak, T. D. Schmittgen, Analysis of relative gene expression data using real-time quantitative PCR and the 2-ΔΔCT method. *Methods* **25**, 402–408 (2001).
63. J. A. Schloss, A Chlamydomonas gene encodes a G protein β subunit-like polypeptide. *Mol. Gen. Genet.* **221**, 443–452 (1990).
64. A. Dobin *et al.*, STAR: Ultrafast universal RNA-seq aligner. *Bioinformatics* **29**, 15–21 (2013).
65. S. Anders, P. T. Pyl, W. Huber, HTSeq–A Python framework to work with high-throughput sequencing data. *Bioinformatics* **31**, 166–169 (2015).
66. M. D. Robinson, D. J. McCarthy, G. K. Smyth, edgeR: A Bioconductor package for differential expression analysis of digital gene expression data. *Bioinformatics* **26**, 139–140 (2009).
67. D. Tolleter *et al.*, Coral bleaching independent of photosynthetic activity. *Curr. Biol.* **23**, 1782–1786 (2013).
68. J. M. Troiano *et al.*, Identification of 1 distinct pH- and zeaxanthin-dependent quenching in LHCSR3 from chlamydomonas reinhardtii. *Elife* **10**, 1–59 (2021).
69. W. Bilger, O. Björkman, Role of the xanthophyll cycle in photoprotection elucidated by measurements of light-induced absorbance changes, fluorescence and photosynthesis in leaves of *Hedera canariensis*. *Photosynth. Res.* **25**, 173–185 (1990).
70. S. Cazzaniga *et al.*, Domestication of the green alga *Chlorella sorokiniana*: Reduction of antenna size improves light-use efficiency in a photobioreactor. *Biotechnol. Biofuels* **7**, 157 (2014).
71. T. De Marchin, B. Ghysels, S. Nicolay, F. Franck, Analysis of PSII antenna size heterogeneity of Chlamydomonas reinhardtii during state transitions. *Biochim. Biophys. Acta* **1837**, 121–130 (2014).
72. U. K. Laemmli, Cleavage of structural proteins during the assembly of the head of bacteriophage T4. *Nature* **227**, 680–685 (1970).
73. M. G. Casabona, Y. Vandenbrouck, I. Attree, Y. Couté, Proteomic characterization of Pseudomonas aeruginosa PAO1 inner membrane. *Proteomics* **13**, 2419–2423 (2013).
74. S. S. Merchant *et al.*, The Chlamydomonas genome reveals the evolution of key animal and plant functions. *Science* **318**, 245–251 (2007).
75. D. Bouyssié *et al.*, Proline: An efficient and user-friendly software suite for large-scale proteomics. *Bioinformatics* **36**, 3148–3155 (2020).
76. Y. Couté, C. Bruley, T. Burger, Beyond target-decoy competition: Stable validation of peptide and protein identifications in mass spectrometry-based discovery proteomics. *Anal. Chem.* **92**, 14898–14906 (2020).
77. S. Wieczorek *et al.*, DAPAR & ProStaR: Software to perform statistical analyses in quantitative discovery proteomics. *Bioinformatics* **33**, 135–136 (2017).
78. P. Albanese, S. Tamara, G. Saracco, R. A. Scheltema, C. Pagliano, How paired PSII–LHCII supercomplexes mediate the stacking of plant thylakoid membranes unveiled by structural mass-spectrometry. *Nat. Commun.* **11**, 1–14 (2020).
79. Z. L. Chen *et al.*, A high-speed search engine pLink 2 with systematic evaluation for proteome-scale identification of cross-linked peptides. *Nat. Commun.* **10**, 3404 (2019).
80. E. M. Holgersen *et al.*, Transcriptome-wide off-target effects of steric-blocking oligonucleotides. *Nucleic Acid Ther.* **31**, 392–403 (2021).
81. R. V. Honorato *et al.*, Structural biology in the clouds: The WeNMR-EOSC ecosystem. *Front. Mol. Biosci.* **8**, 729513 (2021).
82. M. Mirdita *et al.*, ColabFold: Making protein folding accessible to all. *Nat. Methods* **19**, 679–682 (2022).
83. A. T. Kong, F. V. Leprevost, D. M. Avtonomov, D. Mellacheruvu, A. I. Nesvizhskii, MSFragger: Ultrafast and comprehensive peptide identification in mass spectrometry-based proteomics. *Nat. Methods* **14**, 513–520 (2017).
84. Y. Couté, Proteomic characterization of UV-B impact on Chlamydomonas reinhardtii. Proteome Xchange. https://proteomecentral.proteomexchange.org/cgi/GetDataset?ID=PXD048496. Deposited 12 January 2024.
85. P. Albanese, Photoreceptor-induced LHL4 protects photosystem II in Chlamydomonas reinhardtii - BN-PAGE profiling. Proteome Xchange. https://www.ebi.ac.uk/pride/archive/projects/PXD055508. Deposited 13 February 2024.
86. P. Albanese, Photoreceptor-induced LHL4 protects photosystem II in Chlamydomonas reinhardtii. Proteome Xchange. https://www.ebi.ac.uk/pride/archive/projects/PXD049352. Deposited 13 February 2024.
87. R. Ulm, E. Demarsy, M. Dannay, G. Allorent, UV effect on WT, uvr8, CrCo, and CrBlz3 transcriptome. NCBI Gene Expression Omnibus. https://www.ncbi.nlm.nih.gov/geo/query/acc.cgi?acc=GSE255943. Deposited 16 February 2024.
88. P. Albanese, Photoreceptor-induced LHL 4 protects photosystem II monomer – XL-MS and Alphafold2 intergrative modelling. Zenodo. https://zenodo.org/records/14262714. Deposited 2 December 2024.